COBEM 2021 26th International Congress of Mechanical Engineering
November 22-26, 2021, Virtual Congress, Brazil

COB-2021-0995
LONG PULSE THERMOGRAPHY FOR NONDESTRUCTIVE INSPECTION OF AERONAUTICAL MATERIALS

José Jerônimo Rabelo Faria
Alfredo Rocha de Faria
Department of Mechanical Engineering, Instituto Tecnológico de Aeronáutica
Praça Marechal Eduardo Gomes, 50
São José dos Campos, SP, Brazil - 12228-900
jfaria@ita.br, arfaria@ita.br

Abstract. *Infrared Thermography (IRT) is a contactless, rapid Nondestructive Testing (NDT) technique that has received considerable attention over the last years, mainly due to its simplicity and suitability for large-scale inspection of complex structures. IRT can be classified as passive or active, depending on the available control of the thermal radiation source. In passive mode, the object under analysis is naturally at a temperature higher or lower than the environment, creating a measurable thermal contrast on its surface. On the other hand, in active mode, the object is thermally excited by an external source and its thermal response is analyzed. Stimulation sources include optical radiation, ultrasonic wave propagation, eddy current and others. Among the different active thermography techniques, Long Pulse Thermography (LPT) with optical excitation is a cost-effective and promising technique, especially for the inspection of large composite structures. The objective of the present research is to evaluate the performance of the technique combined with computer vision algorithms on both composites and metallic materials. The evaluated LPT system is comprised of an uncooled microbolometer imager with resolution of 382x288 pixels and 2kW halogen lamps. A data set of thermograms from specimens with simulated flaws were collected and used to train a pixel classification model, based on random forests, for automatic image segmentation into defective and sound areas. The model was then evaluated on curved and flat specimens manufactured out of Carbon Fiber Reinforced Polymer (CFRP). Results revealed that the technique can be successfully applied to both materials; however, considerably better performance was achieved on the CFRP samples. Additionally, the proposed pixel classification model achieved a higher degree of accuracy when compared to other automatic segmentation strategies, with accurate identification of defective areas.*

Keywords: *Nondestructive Testing, Infrared Thermography, Image Processing, Aeronautical Structures*

1. INTRODUCTION

The highly competitive airline market landscape is a constant driver for new technologies capable of reducing operational costs and increasing profitability. From an engineering standpoint, this translates into the need for aircraft with longer service lives, shorter inspection downtimes, and longer inspection intervals (Bafekrpour, 2017). Airframe material selection plays a vital role in the Direct Operating Costs (DOC) of an aircraft. This impact is especially pronounced on material costs (raw or semi-finished), manufacturing costs, airframe weight (i.e. payload and fuel consumption), and maintenance (i.e. inspection, repair, and/or replacement) (Ilcewicz; Hoffman; Fawcett, 2000). The latter having recurrent, cumulative impact over the complete life cycle of the aircraft. Therefore, a reduction in structural weight and maintenance requirements can impact the DOC significantly.

Composite materials, particularly Carbon Fiber Reinforced Plastics (CFRP), have played a major role in airframe structural design concepts, allowing for unprecedented advancements in performance. As an example, the Boeing 777 composite empennage is 25% lighter than the Boeing 767 aluminum empennage, yet it requires 35% less scheduled maintenance hours (Hale, 2008). These figures are even more impressive considering the size difference between the aircraft – the Maximum Takeoff Weight (MTOW) of the 777 is over 100,000 kg higher than the 767. Recent advances in composite manufacturing have allowed the industry to significantly increase their application, reflected in their widespread use in modern airliners, such as the Airbus A350XWB (53%) and Boeing 787 (50%) (Smith, 2013). However, despite its many advantages, considerable challenges exist regarding the use of composite materials. One of the unique characteristics of composites is the degree of attention required in the material procurement specification and manufacturing (Bafekrpour, 2017). Consequently, additional Nondestructive Testing (NDT) requirements are imposed in order to provide assurance that the completed structure meets its functional and design requirements (Federal Aviation Administration, 2009).

2. NONDESTRUCTIVE EVALUATION VIA INFRARED THERMOGRAPHY (IRT)

IRT can be considered one of the most promising NDT methods for the inspection of composite structures, mainly due to its non-contact nature, high inspection rate and easy data interpretation (Ciampa et al., 2018). IRT for NDT applications, or simply Thermal NDT (TNDT) (Vavilov; Burleigh, 2015), can be classified as passive or active, depending on the available control of the thermal radiation source. In passive mode, the object under analysis is naturally at a temperature higher or lower than the environment, creating a measurable thermal contrast on its surface. On the other hand, in active mode, the object is thermally excited by an external source and its thermal response is analyzed (Maldague; Marinetti, 1996). Stimulation sources include optical radiation, ultrasonic wave propagation, eddy current and others (Ciampa et al., 2018). TNDT is considered a nonconventional NDT technique, with the fist standard being published in 2007 by ASTM (ASTM International, 2019). Particular attention will be given here to optical TNDT.

2.1 Thermal Properties of Materials

The most general equation governing the temperature variation in a material under thermal stimulus is Cattaneo's equation (Barletta; Zanchini, 1997):

$$Q + t_r \frac{\partial Q}{\partial t} = -\kappa \nabla T \tag{1}$$

where Q is the heat flux, t_r the material's relaxation time, t is time, κ the material's thermal conductivity coefficient and T the temperature.

Considering the conservation of energy (Eq. 2):

$$\frac{1}{V_h^2} + \frac{\partial^2 T}{\partial t^2} + \frac{1}{\alpha}\frac{\partial T}{\partial t} - \nabla^2 T = 0 \tag{2}$$

where V_h and α are the propagation of thermal waves and thermal diffusivity, respectively.

The thermal wave propagation is given by Eq. (3):

$$V_h = \sqrt{\frac{\alpha}{t_r}} \tag{3}$$

So, when $V_h \to \infty$, or $t_r \to 0$ (infinite heat propagation velocity), the classical Fourier's heat conduction equation can be assumed, Eq. (4). This indicates that the static thermal properties of a material generally dictate heat propagation.

$$\frac{\partial T}{\partial t} - \alpha \nabla^2 T = 0 \tag{4}$$

The most relevant thermal properties for the application of TNDT are: emissivity, thermal conductivity, thermal diffusivity, specific heat, and thermal effusivity. Emissivity ε is a surface property that indicates the effectiveness in emitting energy as thermal radiation. It is a ratio between the energy emitted by an object and a perfect emitter (blackbody). High emissivity surfaces are ideal for thermography applications. Thermal conductivity κ indicates the ability of a material to conduct heat, and it depends on the material molecular configuration. Thermal diffusivity measures the ability of a material to conduct and exchange heat. It is the ratio between thermal conductivity divided by density and specific heat capacity. Specific heat c is the measure of energy necessary to raise a unit mass of the material by one degree of temperature. Lastly, thermal effusivity e indicates the ability of a material to exchange heat with its surroundings. It is also related to the thermal conductivity, density, and specific heat.

2.2 Long Pulse Thermography

The most common optically stimulated thermography methods applied to aerospace structures are Pulsed Thermography (PT) and Lock-in Thermography (LIT) (Ciampa et al., 2018; Vavilov; Burleigh, 2015). PT is carried out by providing a heat pulse to the object under evaluation and monitoring its surface temperature under the transient cooling or heating phases. Hence, the technique is also referred to as Transient Thermography (TT). Heating is usually done with flash lamps, but can also be carried out with halogen lamps. In the latter case, the heating requires a longer time, and the technique is called Long Pulse Thermography (LPT) or Step Pulse Thermography (SPT). Figure 1 illustrates the technique and thermal response in the presence of a structural anomaly, such as voids.

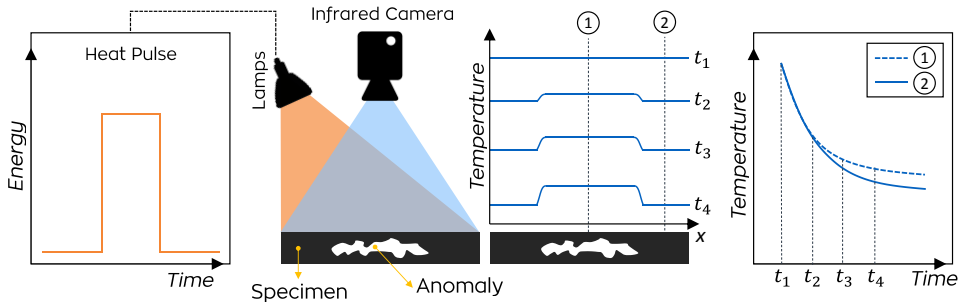

Figure 1. Pulse thermography.

The thermal energy propagates by conduction inside the structure while the infrared camera monitors the temperature variation over the surface. For a uniform surface heating and homogeneous material, the temperature distribution over time is uniform. However, the presence of a subsurface anomaly interferes with the heat flow, due to a localized variation of thermal properties, causing local surface temperature variations, as illustrated in Figure 2. Generally, a shallow defect becomes visible earlier than a deep one and a larger defect produces a more pronounced temperature difference (contrast). Moreover, there are two configurations of thermal camera positioning in relation to the excitation source, named transmission mode and reflection mode. In transmission mode, the thermal camera and the stimulus are on opposite sides of the inspected material, while in the reflection mode, both are located on the same side, as illustrated in Figure 1. Often, in practical applications, accessibility to both sides of a structure is difficult (e.g., aircraft fuselage), making the reflection mode the most attractive.

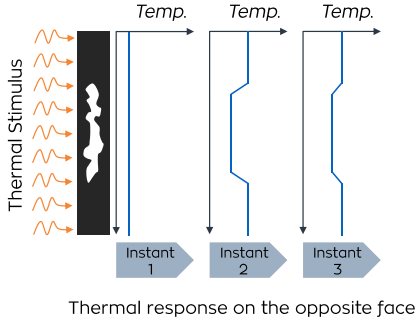

Figure 2. Thermal response in the presence of a subsurface anomaly.

Defect visibility depends on several factors, which include material characteristics, environmental conditions, excitation power, and infrared camera sensitivity. Regarding material characteristics, both thermal properties (thermal conductivity, thermal diffusivity) and defect geometry play key roles (Meola; Carlomagno; Giorleo, 2004). A common metric utilized to evaluate detectability is the Aspect Ratio (AR) of the defect – ratio between the planar size, D, and depth, t, ($AR = D/t$). For a defect to be detected, it is generally considered that its aspect ratio should be greater than 2 (for isotropic materials) (Maldague, 2002). Additionally, another important characteristic of the defect is its thickness. A large radius defect is hard to detect if it is very thin (e.g., kissing bonds); conversely, a thicker defect (e.g., large void) with smaller radius is more easily detectable (Meola; Carlomagno; Giorleo, 2004).

The metric adopted to characterize the performance of the LPT system is the signal-to-noise ratio (SNR). The quantification of the SNR allows the analysis of the relationship between signal strength of a defect and the level of background noise at the maximum signal contrast. The SNR adopted in the present study is given by Eq. 5 (Rodríguez, 2013; Usamentiaga; Ibarra-Castanedo; Maldague, 2018).

$$SNR = \frac{S_d - S_i}{\sigma_i} \tag{5}$$

Where S_d is the pixel intensity at the defect's center (average intensity of a kernel of 5x5 pixels), S_i the pixel intensity at a sound, reference area (average intensity of a circular kernel with approximately 25 pixels in the vicinity of the defect), and σ_i is the standard deviation of the pixel intensity over the sound reference area.

The contour of the defect can be determined by analyzing the temperature T of pixels at the vicinity of the known defect center (point of highest contrast). If a given pixel satisfy both conditions, it is classified as a defective area. This criterion is similar to Z-criterion proposed by Vavilov *et al.* (1998). It can be noticed that the analysis of the thermograms is highly dependent on the choice of sound and defective areas, in other words, it requires a degree of expertise. An

important aspect during analysis is that the reference sound area should be as close as possible to the potential defect. This reduces the influence of nonuniform heating and other noise sources (Rodríguez, 2013).

2.3 Image Processing Techniques

Thermograms obtained using optical stimulation are often contaminated with different noise sources, such as reflected infrared energy from the surroundings, non-homogeneous heating and variations in optical properties of the specimen (Ciampa *et al.*, 2018). These noise sources influence flaw detectability, since they produce abnormal thermal patterns in the images. In order to enhance the contrast between sound and defective areas, a number of signal processing algorithms have been developed (Vavilov; Burleigh, 2015). The most widely used algorithms are grouped in Figure 3. Data from a typical TT analysis consists of a sequence of infrared images (thermograms) that display the surface temperature distribution and evolution in time. This allows for distinct data processing strategies, namely: one-dimensional (temporal), two-dimensional (spatial) or a combination of both. 1D algorithms are applied on a pixel basis and analyze the pixel temperature evolution (image sequence). On the other hand, 2D algorithms are applied to a single image and operate on a pixel-to-pixel basis (e.g., contrast adjustment, filtering, etc.). Most TNDT processing algorithms rely on the pixel temporal evaluation, since more information about defect parameters, such as defect depth, can be obtained (Vavilov; Burleigh, 2015). However, 2D algorithms are fundamental for image segmentation and feature extraction, which are important steps in the implementation of automated image processing algorithms employing machine learning strategies (Szeliski, 2010).

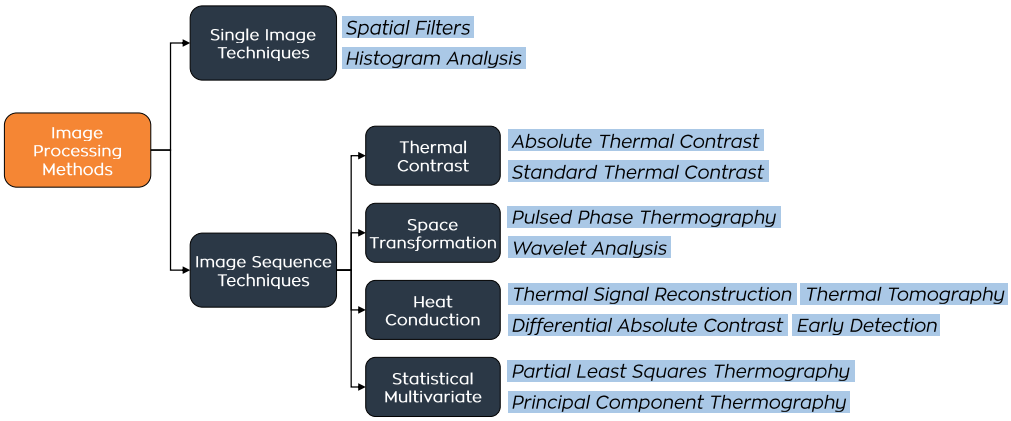

Figure 3. Most widely used image processing algorithms in TNDT (Vavilov; Burleigh, 2015).

Among the different TNDT image processing algorithms, Thermal Signal Reconstruction (TSR) will be used in the present study (Shepard, 2018, 2001). The pre-processed thermograms will be further analyzed using single image techniques, namely spatial filtering, contrast enhancement and segmentation. This was performed with *ilastik*, a free software for interactive image classification, segmentation, and analysis, built originally for bioimage processing. The objective of image segmentation is to obtain a binary image divided in two classes: sound (background) and defect (foreground) areas.

3. MATERIALS AND METHODS

Thermograms of a carbon fiber/epoxy specimens containing simulated flaws were acquired using an in-house LPT system comprised of an uncooled microbolometer imager and halogen optical sources with a total power of 2 kW (See Figure *4*). The infrared sensor operates in the LWIR (Long-Wave Infrared) spectrum, with sensitivity of 80 mK, resolution of 382x288 pixels and 8-bit pixel depth. In addition to the hardware setup, a software package was developed in C++ programming language. The software allows for synchronized operation of the infrared camera and excitation sources. Settings such as acquisition rate, emissivity, excitation and acquisition time can also be configured via a user interface. A total of three specimens were used to evaluate the LPT system, illustrated in Figure 5. The first specimen (A) is a flat plate, manufactured with woven fabric with a total of 25 flat-bottom holes of varying diameter (2-20 mm) and depth (0.5-2 mm), with total thickness of 2.5 mm. The flat-bottom holes were milled following recommendations regarding flaw size and distribution of ASTM 2582-19. The second specimen (B) was manufactured using the same laminate as Specimen A, with a simulated bond line and flat-bottom hole with diameters of 7 mm and 3 mm, with depths of 1.5 mm. The third specimen (C) is a skin section, manufactured using automated tape laying, with a center stringer. Flat-bottom-holes (diameter of 10 mm and 1.5 mm depth) were milled on both sides of the specimen and a lateral hole (3 mm in diameter and 40 mm in length) was drilled in the stringer base, to simulate a discontinuity between skin and reinforcement.

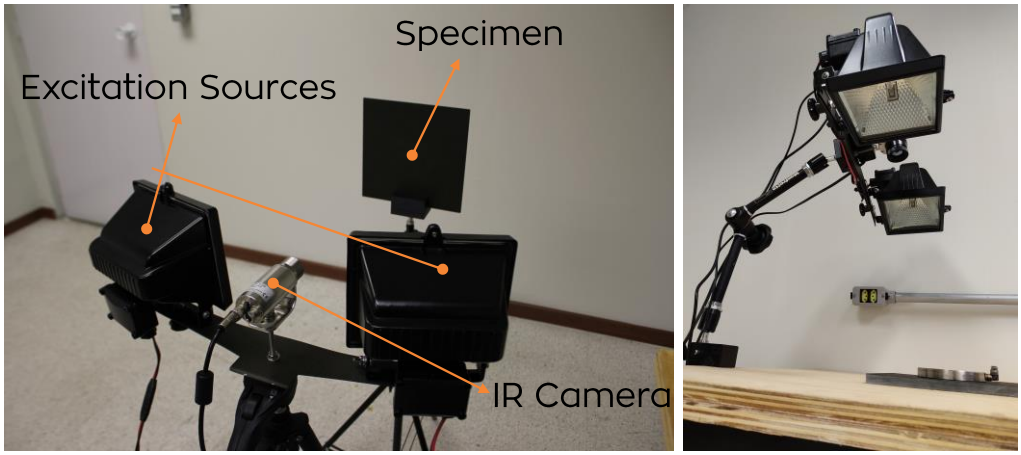

(a) (b)

Figure 4. In-house LPT system in a tripod (a) and tabletop (b) setup.

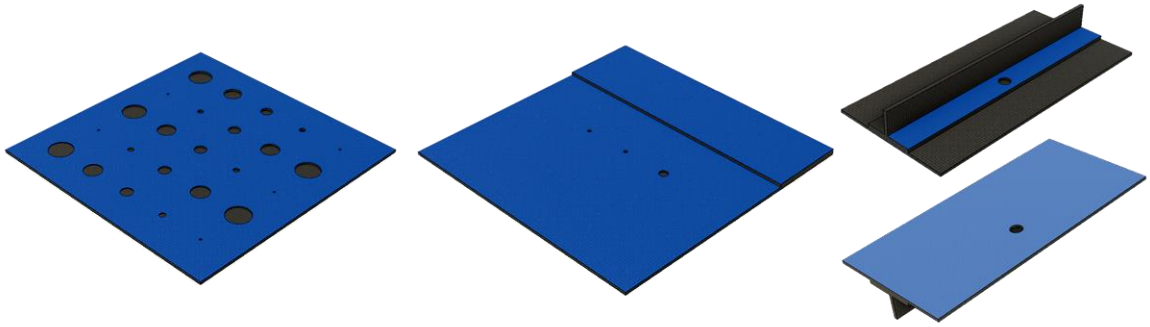

Figure 5. Specimens A, B and C, from left to right.

4. RESULTS

The first tests were conducted to investigate the effect of the heating time on defect contrast and SNR. For this analysis, Specimen A was utilized, since it has multiple simulated flaws with varying aspect ratios. A fixed inspection distance of 50 cm was used, yielding a pixel resolution of 0.71 mm. Four heating times were analyzed: 5, 10, 15 and 20 seconds. After the heating pulse, data was acquired at 30 frames per second, for a period equivalent to double the heating time – for 5 seconds of heating time, 10 seconds of acquisition time, and so forth.

Figure 6 illustrates the difference in contrast between a raw thermogram and the same thermogram pre-processed with the TSR algorithm. Despite being extensively used for Flash Thermography, the results support that the algorithm also produces good results for LPT, with the 1st Derivative yielding the best contrast. The 2nd Derivative image increases the contrast in certain instants of time, but in general terms does not outperform the raw data, as supported by (Rodríguez, 2013). For this reason, the 1st Derivative images were used for the subsequent analysis.

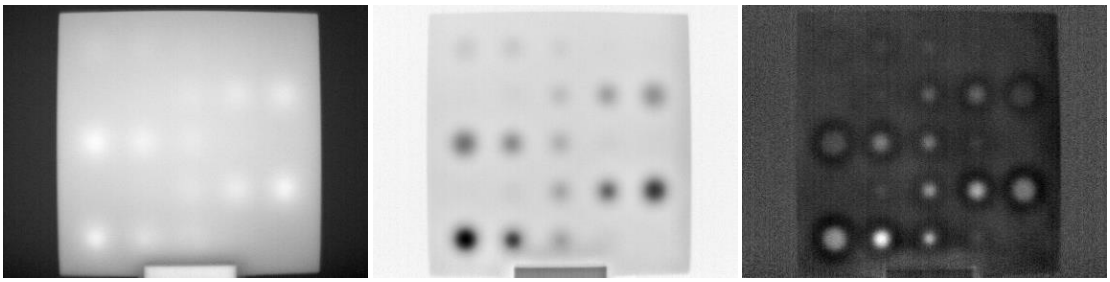

(a) (b) (c)

Figure 6. Comparison between raw (a), TSR 1st Derivative (b) and TSR 2nd Derivative (c) thermograms of the same instant of time.

The flat-bottom holes with 20 mm diameters were used to analyze the behavior of the SNR for the different heating times (See Figure 7). It is possible to notice a considerable increase in the SNR between the tests with 5 seconds and 10 seconds of heating pulse, for all the ARs, with the exception of the defect with AR = 10 (2 mm depth), which presented a similar response for all heating times. The SNR performance for 15 and 20 seconds was similar to that of 10 seconds, with a slight decrease in SNR observable for 20 seconds. This suggests that the optimum excitation time for the equipment is between 10 and 15 seconds. Longer heating pulses yield higher surface temperature; however, the contrast between defect and sound areas is not necessarily increased, as the surface temperature tends to reach a homogeneous state. This is due to the different heating transfer mechanisms taking place during the inspection. Moreover, it is possible to notice that the shallower defects appear with greater contrast in the early thermograms, while deeper defects appear later. The images also reveal that the defects with diameter of 2 mm cannot be detected, even at 0.5 mm depth (AR = 4). Defects at 2 mm depth also present very weak contrast, even for larger diameters.

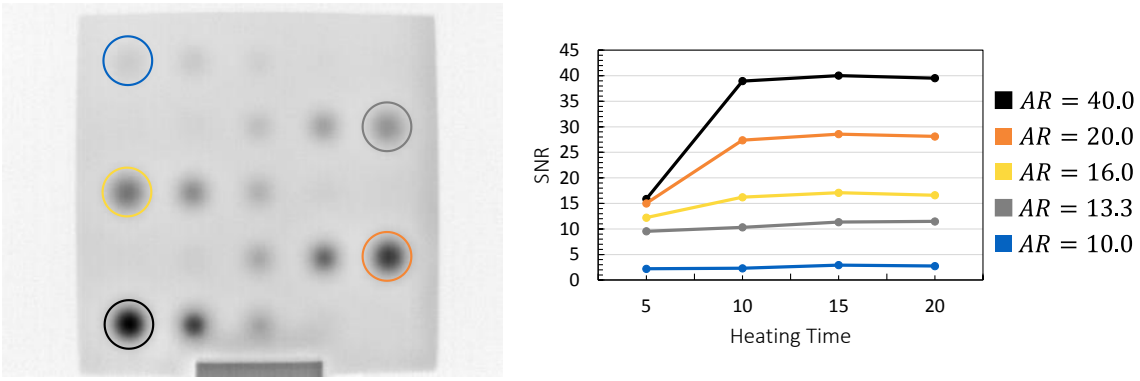

Figure 7. SNR for the 20 mm flat-bottom holes at different depths, for different heating times.

Results obtained with Specimen B, shown in Figure 8, reveal the great capability of LPT to detect bond line flaws. Despite the greater depth (2.5 mm), the bond line can be observed with great contrast, highlighting the regions with voids and discontinuities. The flat-bottom holes could also be detected, even the ones with 3 mm in diameter.

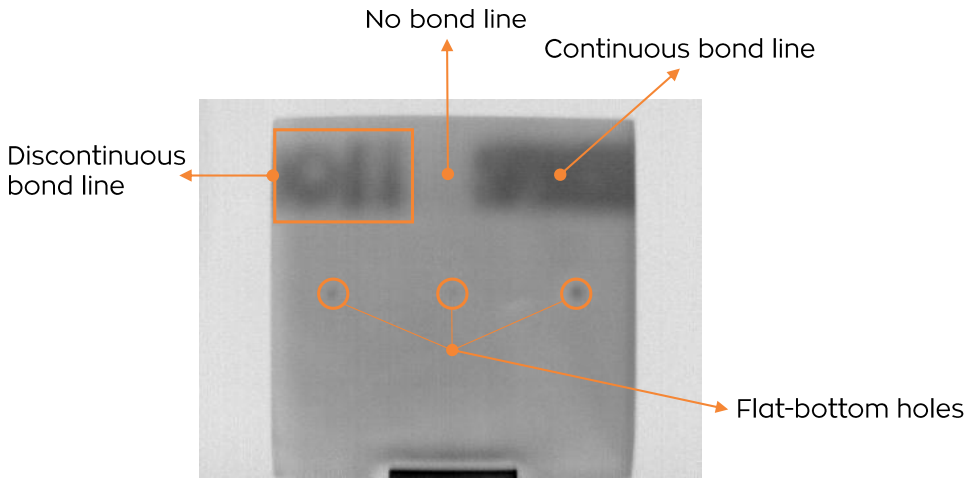

Figure 8. 1st Derivative image of Sample B, highlighting the simulated bond line and flat-bottom holes.

Tests with Specimen C revealed that the FBHs could not be detected from either side. The lateral hole was detected; however, with poor SNR. The stringer base appears with good definition, as well as the bond line (See Figure 9). This specimen did not have simulated voids between the string and base plate; however, the results reveal that the equipment would be capable of detecting this kind of defect with good accuracy, as supported by the results obtained with Specimen B.

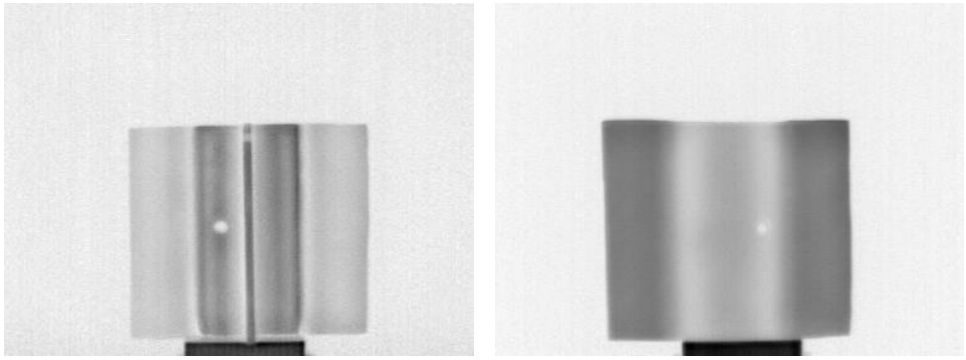

(a) (b)

Figure 9. TSR 1st Derivative images of Specimen C, front face (a) and back face (b). The visible flat-bottom holes in both images are in the inspected surface.

The best results obtained with the experiments with Specimen A were used to train a pixel classification algorithm using *ilastik*. The procedure is straightforward and consists of selecting sample images in the software interface for feature annotation. The utilized features were Color/Intensity, Edge and Texture. Different levels of low-pass filtering (blur) were also used, ranging from σ equal to 0.3 to 10. This enriches the data set and aids extrapolations. A total of 30 thermograms extracted from the image sequence acquired during transient cooling were used to train the classifier. The classifier was then evaluated on thermograms of Specimen A and B (See Figure 10). Results show that the classification algorithm can successfully segment the image into defective (blue) and sound (yellow) areas. However, considerable noise is present in the image, especially in the edges of the plates. Further pre-processing with denoising algorithms, such as homogenization and subtraction, may aid pixel classification. Nevertheless, the false positive regions can be easily distinguished from the defects, since they appear in the edges and with lower intensity.

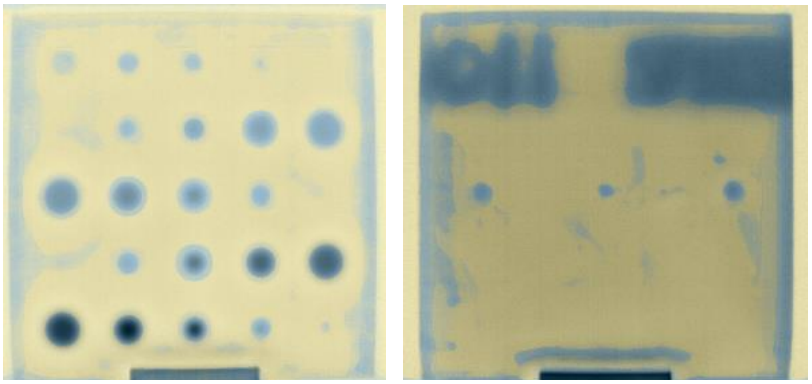

Figure 10. Output of the pixel classification algorithm trained using *ilastik*, superimposed over the original gray scale thermograms, for Specimen A (left) and Specimen B (right).

5. CONCLUSIONS

The present study evaluated the performance of an in-house LPT system for the inspection of carbon-epoxy samples, utilized in the aeronautical industry. Results revealed that the technique is capable of detecting simulated defects of several aspect ratios, with especially good results in the detection of bond lines. The system was also evaluated for the inspection of a complex reinforced plate. Moreover, a pixel classification framework based on *ilastik* was trained to automatically segment images into defect and sound areas. The *ilastik* software showed good potential for image processing in TNDT, with easy implementation and accurate results. In future developments, a larger data set should be used for training, exploring different defects and specimen geometries.

6. ACKNOWLEDGEMENTS

The authors would like to acknowledge the Brazilian funding agencies CNPq and FAPESP for the grants CNPq 306193/2017-5, 163101/2017-5 and FAPESP 2019/00917-8, that supported this research.

7. REFERENCES

ASTM E2582-19. Standard Practice for Infrared Flash Thermography of Composite Panels and Repair Patches Used in Aerospace Applications. [s.l.] ASTM International, 2019. Disponível em: <www.astm.org>.

Bafekrpour, E. Advanced Composite Materials: Properties and Applications. [s.l.] De Gruyter Open Poland, 2017.

Barletta, A.; Zanchini, E. Hyperbolic Heat Conduction and Local Equilibrium: A Second Law Analysis. International Journal of Heat and Mass Transfer, v. 40, n. 5, p. 1007–1016, mar. 1997.

Ciampa, F. et al. Recent Advances in Active Infrared Thermography for Non-Destructive Testing of Aerospace Components. Sensors, v. 18, n. 2, p. 609, 16 fev. 2018.

Federal Aviation Administration. Quality System for the Manufacturing of Composite Structures. [s.l: s.n.].

Hale, J. Boeing 787: From the Ground Up. Disponível em: <www.boeing.com>.

Ilcewicz, L. B.; Hoffman, D. J.; Fawcett, A. J. Composite Applications in Commercial Airframe Structures. In: Comprehensive Composite Materials. [s.l.] Elsevier, 2000. p. 87–119.

Maldague, X. Introduction to NDT by Active Infrared Thermography. Materials Evaluation, v. 6, p. 1060–1073, 2002.

Maldague, X.; Marinetti, S. Pulse Phase Infrared Thermography. J. Appl. Phys., v. 79, n. 5, p. 6, 1996.

Meola, C.; Carlomagno, G. M.; Giorleo, L. Geometrical Limitations to Detection of Defects in Composites by Means of Infrared Thermography. Journal of Nondestructive Evaluation, v. 23, n. 4, p. 125–132, dez. 2004.

Rodríguez, F. De J. L. Detection and Characterization of Subsurface Defects by Infrared Pulsed Thermography. [s.l.] Federal University of Santa Catarina, 2013.

Shepard, S. Active Thermography for NDT. In: CONAENDI. São Paulo, Brazil, 2018.

Shepard, S. M. Advances in Pulsed Thermography. (A. E. Rozlosnik, R. B. Dinwiddie, Eds.). In: Aerospace/Defense Sensing, Simulation, And Controls. Orlando, FL: 23 mar. 2001.

Smith, F. The Use of Composites in Aerospace: Past, Present and Future Challanges, 2013.

Szeliski, R. Computer Vision: Algorithms and Applications. p. 979, 2010.

Usamentiaga, R.; Ibarra-Castanedo, C.; Maldague, X. More than Fifty Shades of Grey: Quantitative Characterization of Defects and Interpretation Using SNR and CNR. Journal of Nondestructive Evaluation, v. 37, n. 2, p. 25, jun. 2018.

Vavilov, V. P.; Burleigh, D. D. Review of Pulsed Thermal NDT: Physical Principles, Theory and Data Processing. NDT & E International, v. 73, p. 28–52, jul. 2015.

8. RESPONSIBILITY NOTICE

The authors are the only responsible for the printed material included in this paper.